PCCP
Physical Chemistry Chemical Physics

Accepted Manuscript

This article can be cited before page numbers have been issued, to do this please use: N. Watanabe, S. Arakaki and M. Takahashi, *Phys. Chem. Chem. Phys.*, 2026, DOI: 10.1039/D6CP00868B.

ROYAL SOCIETY OF CHEMISTRY

rsc.li/pccp

View Article Online
DOI: 10.1039/D6CP00868B

ARTICLE

Molecular conformation of dimethyl oxalate studied by electron momentum spectroscopy

Noboru Watanabe,[a] Shota Arakaki [a] and Masahiko Takahashi *[a]

Received 00th January 20xx,
Accepted 00th January 20xx

DOI: 10.1039/x0xx00000x

The shapes of molecular orbitals convey conformational information about the molecule. Electron momentum spectroscopy (EMS) is a method that measures individual molecular orbitals in the momentum space, and it may thus offer a tool for examining molecular conformation that cannot be fully determined by conventional structure-analysis techniques. In consideration of this, EMS measurements were conducted on dimethyl oxalate, the molecular structure of which in the gas phase has long been the subject of considerable debate. The obtained momentum profiles were found to be unexplained by theoretical calculations with a fixed CC torsional angle, φ. The deviations from the experiment were almost resolved by incorporating the influence of thermal-induced CC torsional motion, inferred from theoretical potential energy curves (PECs) along φ. The findings demonstrate that the CC torsional angle is distributed over the entire range from 0° to 180° at room temperature. Furthermore, the energy of the *trans*-structure is revealed to be lower than that of the *cis*-structure. For the highest occupied orbital, a small but discernible variation was observed in the theoretical momentum profile, depending on the PEC used. A theoretical analysis reveals that the PEC dependence is enhanced by decreasing the temperature, indicating that EMS experiments at low temperatures may provide a valuable opportunity to examine the torsional potential, whose reliable theoretical prediction has been hindered by the delicate balance between π bonding effects and lone pair-lone pair repulsion.

Introduction

An accurate understanding of molecular structure is imperative for discussing molecular reactivity and functionality at the atomic scale. Consequently, precise structural analysis has been performed on numerous molecules using various techniques, such as x-ray and electron diffraction, microwave spectroscopy, vibrational spectroscopy, and nuclear magnetic resonance. Nevertheless, there are still molecules whose precise structures remain undetermined. Dimethyl oxalate is an example of such a molecule. Its molecular structure consists of two methyl carboxylate groups linked by a CC bond (see Fig. 1), and as demonstrated by the x-ray crystallographic studies, [1,2] dimethyl oxalate is confirmed to exist in the planar *trans*-conformation with C_{2h} symmetry in the solid phase. Conversely, the conformational properties of the molecule in the gas and liquid phases have been the subject of debate since the 1940s. [3-9]

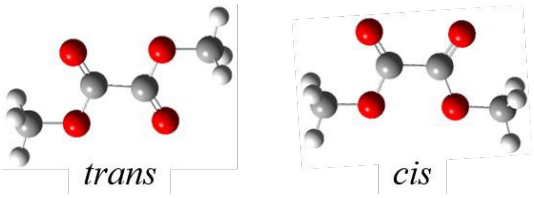

Fig. 1 Planar *trans*- and planar *cis*-conformations of dimethyl oxalate.

The infrared (IR) and Raman spectra of dimethyl oxalate in the solid phase have been shown to exhibit significant disparities from those in other phases.[3-6] In order to account for these observations, several hypotheses concerning the conformation in the gas and liquid phases have been proposed. In the early studies, the coexistence of *trans*- and *cis*-conformers was postulated by Saksena [3] and Miyazawa. [4] In contrast, Wilmshurst and Horwood [5] proposed that the molecule possesses a single nonplanar structure with C_2 symmetry, wherein the constituent carboxylate groups are rotated by ~40° relative to the planar *trans*-conformation about the central CC bond. A reexamination of the IR and Raman spectra led Durig and Brown [6] to a different conclusion that the primary skeleton of the molecule is in the planar *trans*-configuration in both the solid and liquid phases; however, the methyl groups exhibit a rotation away from the plane in the melting process. The infrared spectroscopy study by Katon and Lin [7] concluded that dimethyl oxalate in the liquid exists as a mixture of two conformational equilibria, one of which is the planar *trans*-structure. In a more recent study, Lopes *et al.* [8] measured the IR spectra of dimethyl oxalate isolated in a low-temperature argon matrix and in solid amorphous layers, and also performed potential energy calculations. Based on the experimental and theoretical results, they demonstrated that the large-amplitude torsional vibration around the CC bond in the *trans*-conformation provides a rational explanation for the differences observed in the vibrational spectra between the crystal and other phases. Later, Vishnevskiy *et al*. [9] conducted a gas electron diffraction (GED)

[a] *Institute of Multidisciplinary Research for Advanced Materials, Tohoku University, Sendai 980-8577, Japan. E-mail: masahiko@tohoku.ac.jp*

View Article Online
DOI: 10.1039/D6CP00868B

experiment at a temperature of 323 K in conjunction with quantum chemistry calculations. The experimental outcome was subsequently analyzed using a dynamical model in which 20 pseudo-conformers with varying CC torsional angles were utilized. The analysis yielded a conclusion that *cis*- and *trans*-conformers separated by a low barrier of 0.44 kcal/mol coexist in the gas phase, with the *cis*-conformer being 0.02 kcal/mol lower in energy than the *trans*-conformer. The findings of the IR and GED studies by Lopes *et al.* and Vishnevskiy *et al*., as well as their potential energy calculations, indicate that the conformational problem of dimethyl oxalate can be reduced to a consideration of the CC torsional angle. However, a discrepancy persists among the conclusions of these studies, even regarding the question of whether the *cis*- or *trans*-structure is more stable, and further study is thus necessary.

The shapes of molecular orbitals are contingent upon the molecular structure, thereby imparting conformational information. Given the distribution of individual orbitals over distinct molecular sites, it is conceivable that certain molecular orbitals may exhibit a considerable degree of sensitivity to a structural parameter of interest. Electron momentum spectroscopy (EMS) is an experimental technique that facilitates the measurement of molecular orbital shapes in the momentum space by means of electron Compton scattering. [10-12] In view of the aforementioned considerations, EMS can offer a promising approach for acquiring molecular-structure information that is challenging to extract from other structure-analysis techniques. The sensitivity of EMS to molecular structure has indeed been demonstrated in the investigations on interreference structure that appears in electron momentum distributions [13-16] and in the analysis of conformer abundances for several molecules. [17-23] In the latter studies, the electron momentum distributions of individual orbitals, referred to as momentum profiles, are theoretically calculated for pre-known stable conformers. The abundance ratios are then determined so that experimental momentum profiles are most reproduced by a weighted sum of the theoretical predictions of each conformer. The extension of this approach has a potential to enable the application of EMS to the conformational study of a molecule, even in cases where the equilibrium conformers are not known beforehand, as is the case with dimethyl oxalate.

In this study, an EMS experiment has been performed on dimethyl oxalate to obtain information about the molecular conformation in the gas phase, with a particular focus on the torsional angle around the central CC bond. To this end, the valence orbital momentum distributions are obtained from the experiment, and the results are then compared with theoretical momentum profiles calculated at different torsional angles. It has been demonstrated that the experimental outcomes are not adequately reproducible when a fixed single torsional angle is assumed. A detailed analysis of the data reveals that the CC torsional angle ranges from 0° to 180° at room temperature due to large-amplitude internal rotation, and also that the *trans*-structure is more stable in energy than the *cis*-structure. Furthermore, it is shown that EMS experiments at low temperature can serve as a valuable tool for examining CC torsional potentials, which are recognized as playing an important role in the dynamical mechanisms of various chemical reactions.

Methods

Experimental

EMS is an electron-impact ionization experiment that measures the energies and momenta of the scattered and ejected electrons generated under the high-energy Bethe ridge conditions. [10-12] In this instance, the ionization process is initiated by the collision of the incoming electron with a bound target electron, while the residual ion acts as a spectator. The binding energy E_{bind} and the momentum $\boldsymbol{p}$ of the target electron prior to the ionization can thus be determined through the simple application of the energy and momentum conservation laws between the projectile and target electrons. In accordance with the plane wave impulse approximation (PWIA), the triple-differential cross section of the electron impact ionization is proportional to the electron momentum profile expressed as follows: [10-12]

$$M(p) = \rho_\alpha(p;\boldsymbol{Q}) = \frac{S_\alpha}{4\pi}\int |\psi_\alpha(\boldsymbol{p};\boldsymbol{Q})|^2 d\Omega_{\boldsymbol{p}}\,, \qquad (1)$$

and it provides the spherically-averaged momentum density distribution of the target electron, $\rho_\alpha(p;\boldsymbol{Q})$, with $\boldsymbol{Q}$ being the molecular geometry at the moment of the electron collision. Here p is the magnitude of the target electron momentum $|\boldsymbol{p}|$, S_α represents the spectroscopic factor, and $\psi_\alpha(\boldsymbol{p};\boldsymbol{Q})$ denotes the momentum-space representation of the normalized Dyson orbital. The averaging over the orientation of $\boldsymbol{p}$, $(4\pi)^{-1}\int d\Omega_{\boldsymbol{p}}$, is taken due to the random orientation of the gaseous target molecules. It has been demonstrated that in most cases, the Dyson orbital for outer valence ionization can be adequately represented by the Hartree-Fock or Kohn-Sham orbital to which the target electron belonged before the ionization, and EMS allows for the measurement of the molecular-orbital shape in momentum space.

A concise overview of the EMS spectrometer utilized is provided herein, as the details of the instrument have been thoroughly delineated in other documents. [24] The generation of an electron beam by an electron gun is followed by its intersection with molecular beams effused from multi-nozzles. The resultant ionization of the molecule leads to the ejection of scattered and ejected electrons. Two outgoing electrons which possess nearly identical energies and scattering polar angles of 45° are dispersed by a spherical analyzer prior to reaching position-sensitive detectors. The azimuthal angles of electrons that pass through the analyzer are maintained, thus facilitating the determination of the energies and the emission angles of the outgoing electrons from their arrival positions at the detectors. In this experimental geometry, p is expressed as a function of the azimuthal angle difference between the electrons that are detected in coincidence, $\Delta\phi$. The p

View Article Online
DOI: 10.1039/D6CP00868B

dependence of the electron-impact ionization cross section can thus be determined through the measurement of the electron coincidence counts against $\Delta\phi$.

EMS measurements on dimethyl oxalate were conducted using an incident electron energy of E_0 = 1.2 keV. The experiment did not necessitate the heating of dimethyl oxalate (Tokyo Chemical Industry Co. Ltd., > 99.0 %), a powder sample, due to its sufficient vapor pressure at room temperature. The experimental data were collected over the course of one and half months under an ambient sample pressure of 2 ×10^{-4} Pa. To achieve a higher energy resolution, the outgoing electrons were decelerated with an energy ratio of 1/2.7 before entering the spherical analyzer. The resulting resolutions for E_{bind} and p were, respectively, 1.7 eV full width at half maximum and ~0.16 a.u. at p = 1.0 a.u.

Theoretical calculations

As previously stated, the present study primarily focuses on the mutual angle around the CC bond between the two methyl carboxylate groups, which is represented by the O=C-C=O dihedral angle, φ. The geometries with φ = 180° and 0° correspond to the planar *trans*- and planar *cis*-geometries, respectively. In numerous instances, *ab-initio* calculations have been employed to identify stable conformers of molecules. However, it has been demonstrated that for dimethyl oxalate, the potential energy curve along the O=C-C=O torsional coordinate exhibits significant variation depending on the theoretical methods employed, [8,9] which prevents the reliable determination of equilibrium conformers from theory. The theoretical electron momentum profiles of the molecule were thus calculated for a series of molecular geometries with different φ's for comparison with experiment. To this end, the geometry optimization of the molecule was conducted at the level of second-order Møller–Plesset perturbation theory (MP2) with fixing φ to a specific value. Subsequently, the Kohn-Sham (KS) orbitals were calculated at the optimized geometry employing the Becke-3-parameters-Lee-Yang-Parr (B3LYP) functional, [25,26] and in accordance with the target KS approximation, [27] the electron momentum profiles at the given φ were obtained from the KS orbitals using the HEMS program developed by Brion and his colleagues. [28] For outer valence ionization, the spectroscopic factor is generally close to unity; thus, S_α was set to one. The geometry optimizations and the density functional theory (DFT) calculations were performed with the Gaussian16 program. [29] The Dunning's augmented correlation-consistent polarization valence basis of triple-zeta quality (aug-cc-pVTZ) [30,31] was used in the calculations.

Eqn (1) presupposes that the constituent atoms are fixed at a geometry represented by $\boldsymbol{Q}$. However, recent EMS studies have demonstrated that the changes in the nuclear positions due to internal molecular vibration may considerably influence on the momentum profiles. [32-38] To incorporate this vibrational effect, additional calculations were carried out with the harmonic analytical quantum mechanical (HAQM) approach. [32-34] Within this method, the electron momentum profile is approximately expressed as

$$M(p) = \rho_\alpha(p,\boldsymbol{Q}_0) + \sum_{\text{v}} P_{\text{v}}(T) \sum_{\text{L}} \left\langle \xi_{\text{vL}}(Q_{\text{L}}) \,\middle|\, \rho_\alpha\left(p,\boldsymbol{Q}_0 + Q_{\text{L}}\hat{\boldsymbol{q}}_{\text{L}}\right) - \rho_\alpha(p,\boldsymbol{Q}_0) \,\middle|\, \xi_{\text{vL}}(Q_{\text{L}}) \right\rangle, \quad (2)$$

where $\boldsymbol{Q}_0$ is the equilibrium geometry and $\xi_{\text{vL}}(Q_{\text{L}})$ denotes the harmonic oscillator function of the L-th normal mode, in which the constituent atoms change their positions along a unit vector that indicates the direction of the corresponding normal coordinate, $\hat{\boldsymbol{q}}_{\text{L}}$. The population of the vibrational level at temperature T, denoted as $P_{\text{v}}(T)$, is assumed to be the Boltzmann distribution. The second term on the right-hand side of the equation delineates the influence of molecular vibration and is represented as the sum of terms, each corresponding to the contribution from a single vibrational mode.

In the HAQM calculations, the normal mode analysis was performed at the level of MP2 with the aug-cc-pVTZ basis set (MP2/aug-cc-pVTZ) following the above stated geometry optimizations wherein the value of φ was fixed. Subsequently, the momentum profiles were calculated in accordance with eqn (2), assuming room temperature (T = 298 K). The lowest vibrational mode corresponds to the torsional vibration around the CC bond, and its normal coordinate is practically along φ. In the normal mode analysis, the frequency of this torsional vibration cannot be obtained except at φ = 13° and 180° where the MP2/aug-cc-pVTZ calculation predicts a minimum of the energy. Thus, the contribution of the CC torsional vibration was excluded from the calculations; its influence will be discussed later. The remaining vibrational modes were treated within the harmonic approximation, with the exception of two methyl torsional modes with large anharmonicity, whose influence was inferred in a manner analogous to a method described elsewhere. [39,40] The vibrational effect on the momentum profiles (the second term of eqn (2)) at φ = 180° was calculated with two types of basis sets: valence triple zeta quality, aug-cc-pVTZ, and valence double zeta quality, aug-cc-pVDZ. [30,31] The obtained results were found to be highly consistent with each other; thus, the second term of eqn (2) at other angles was obtained at the B3LYP/aug-cc-pVDZ level to reduce the computational costs, while the first term was calculated at the B3LYP/aug-cc-pVTZ level. The theoretical momentum profiles obtained based on eqn (2) are henceforth referred to as vibrational effects calculations, while those based on eqn (1) with $\boldsymbol{Q}$ of the optimized geometry are denoted as the equilibrium geometry calculations.

To facilitate the attribution of the ionization bands, the vertical ionization energies at the planar *trans*- and planar *cis*-conformations were calculated using the equation-of-motion coupled-cluster singles and doubles for ionization potentials (IP-EOM-CCSD) method [41] with the cc-pVDZ basis set. The calculations were executed using the GAMESS program, [42] and the results are presented in Table I, along with the experimental values reported in a photoelectron spectroscopy study. [43] The differences in the orbital energies between the *trans*- and *cis*-geometries are small, amounting to less than the Franck-

View Article Online
DOI: 10.1039/D6CP00868B

Condon widths observed in the photoelectron spectrum.[43] This suggests that the ionization energies lack sufficient sensitivity to φ to discern the molecular conformation.

Table I Vertical ionization potentials (IPs) calculated at the IP-EOM-CCSD level of theory.

trans		*cis*		Expt.[43]
State	IP (eV)	State	IP (eV)	IP (eV)
$13a_g^{-1}$	9.93	$13a_1^{-1}$	10.36	10.30
$3a_u^{-1}$	11.11	$12b_2^{-1}$	10.98	11.42
$3b_g^{-1}$	11.41	$3a_2^{-1}$	11.11	11.74
$12b_u^{-1}$	11.74	$3b_1^{-1}$	11.44	
$12a_g^{-1}$	12.89	$11b_2^{-1}$	13.10	13.17
$11b_u^{-1}$	13.26	$12a_1^{-1}$	13.26	13.48
$2b_g^{-1}$	13.52	$2a_2^{-1}$	13.52	
$11a_g^{-1}$	14.66	$2b_1^{-1}$	14.79	14.56
$2a_u^{-1}$	14.76	$11a_1^{-1}$	14.88	14.89
$10b_u^{-1}$	15.84	$10b_2^{-1}$	15.77	
$10a_g^{-1}$	16.09	$9b_2^{-1}$	15.95	16.4
$1b_g^{-1}$	16.46	$1a_2^{-1}$	16.46	
$9b_u^{-1}$	16.57	$10a_1^{-1}$	16.73	16.8
$1a_u^{-1}$	17.03	$1b_1^{-1}$	17.05	
$9a_g^{-1}$	18.07	$9a_1^{-1}$	18.35	18.7

Results and discussion

Binding energy spectrum

In the planar *trans*-geometry, dimethyl oxalate belongs to the C_{2h} point group. According to the IP-EOM-CCSD calculation, the outer-valence electron configuration of the molecule can be expressed as follows:

$$(9a_g)^2(1a_u)^2(9b_u)^2(1b_g)^2(10a_g)^2(10b_u)^2(2a_u)^2(11a_g)^2$$
$$(2b_g)^2(11b_u)^2(12a_g)^2(12b_u)^2(3b_g)^2(3a_u)^2(13a_g)^2.$$

The orbital designations in the C_{2h} geometry are to be used henceforth.

Figure 2 presents the binding energy spectrum of dimethyl oxalate, derived by plotting the number of electron-electron coincidence events against the binding energy of the target electron. The separation of the individual ionization bands has been accomplished through a deconvolution process, in which the profile of each ionization band is represented by a Gaussian function. The center position and width of the Gaussian functions were determined from the photoelectron spectrum with high energy resolution, [43] in conjunction with the instrumental energy resolution, and their heights were utilized as the sole fitting parameters to reproduce the experimental spectrum. The same fitting procedure was applied to the ionization spectra at each $\Delta\phi$. By plotting the areas under the Gaussian curves against p, the momentum profiles of the three lowest ionization bands were obtained. The first band is associated with the ionization from the highest occupied molecular orbital (HOMO), $13a_g$, while the second band is formed by ionizations from the close-lying $3a_u$, $3b_g$, and $12b_u$ orbitals (denoted as $\{3a_u + 3b_g + 12b_u\}$, hereafter). The third band is constituted by ionizations from the subsequent three orbitals, $12a_g$, $11b_u$, and $2b_g$, referred to as $\{12a_g + 11b_u + 2b_g\}$ below.

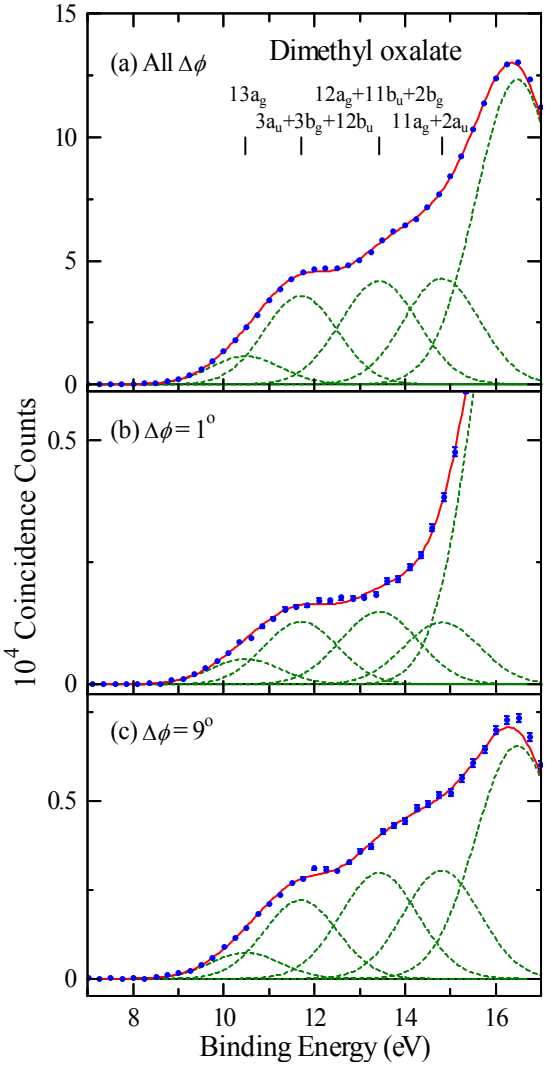

Fig. 2 The binding energy spectra of dimethyl oxalate for (a) the sum of the entire $\Delta\phi$ region covered by the experiment as well as at (b) $\Delta\phi = 1°$ and (c) $\Delta\phi = 9°$. The dashed curves in the figure represent the deconvolution functions, with each curve corresponding to a specific ionization band, and the sum of these functions is depicted by a solid line.

Momentum profiles

Figure 3 presents the experimental momentum profiles thus obtained, along with the vibrational effects calculations at geometries with representative φ values of 0°, 90°, and 180°. Moreover, a comparison is made between the vibrational effects and equilibrium geometry calculations at $\varphi = 0°$ and 180° in the right panels of the figure. The comparison reveals that, while molecular vibration exerts relatively minor effects on the momentum profiles of the $13a_g$ and $\{3a_u + 3b_g + 12b_u\}$ orbitals, the influences are not negligible for quantitative discussions. Furthermore, the vibrational effects calculation for the $\{12a_g + 11b_u + 2b_g\}$ momentum profile predicts significantly higher

View Article Online
DOI: 10.1039/D6CP00868B

intensity at low momentum compared to the equilibrium geometry calculation, indicating the crucial importance of incorporating the vibrational effect in order to accurately interpret the experimental result of the third band. These tendencies have been observed for all CC torsional angles at which the calculations were performed.

As demonstrated in Fig. 3, the theoretical momentum profile of the $13a_g$ orbital exhibits a notable φ dependence. This orbital is predominantly composed of O 2p orbitals in the C=O sites in conjunction with the C-C bonding electron distribution, and its momentum profile is shown to be highly sensitive to φ. Despite the predominant maximum being observed at $p \sim 0.8$ a.u. in the experiment, the calculation assuming $\varphi = 180°$ has predicted the presence of the maximum intensity at $p = 0$. This discrepancy clearly indicates that the molecular structure in the gas phase is different from the planar *trans*-geometry of the molecule in the crystal. Deviation from the experiment is also evident at $\varphi = 0°$ and 90°, and the same is true for other angles. The experimental momentum profile has not been adequately reproduced by the calculation assuming any fixed φ value.

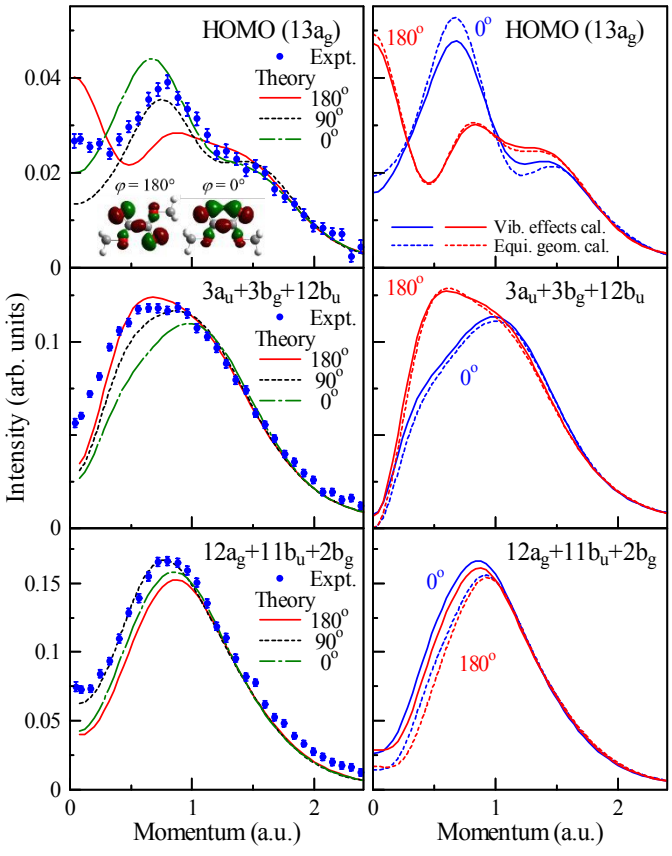

Fig. 3 Experimental and theoretical momentum profiles of the outer valence orbitals of dimethyl oxalate. The left panels compare the experimental results with the vibrational effects calculations at $\varphi = 0°$, 90°, and 180°, all of which are folded with the instrumental momentum resolution. The right panels present comparisons between the vibrational effects and equilibrium geometry calculations at $\varphi = 0°$and 180° without the influence of the instrumental resolution. The inset in the upper left panel presents the theoretical images of the $13a_g$ orbital at $\varphi = 180°$and 0°.

Discernible alternations in the theoretical momentum profiles with φ are also observed for the $\{3a_u + 3b_g + 12b_u\}$ and $\{12a_g + 11b_u + 2b_g\}$ orbitals, while the φ dependences are smaller in comparison to the case of the $13a_g$ orbital. The experimental result of the $\{3a_u + 3b_g + 12b_u\}$ orbital shows a reasonable agreement with the calculation when φ is set to 180°. Conversely, for the $\{12a_g + 11b_u + 2b_g\}$ orbital, a discernible discrepancy emerges between the experiment and the calculation with $\varphi = 180°$, and the former aligns closely with the calculations at $\varphi = 90°$. It is evident that, given a fixed O=C-C=O dihedral angle, no theoretical results have been obtained that reproduce both sets of experimental results for the $\{3a_u + 3b_g + 12b_u\}$ and $\{12a_g + 11b_u + 2b_g\}$ orbitals. The findings indicate that molecular conformations with different φ values contribute to the experimental results. In early studies, [3,4] the coexistence of *trans*- and *cis*-conformers was postulated to explain the appearance of infrared- and Raman-bands that are forbidden for the planar *trans*-conformation. However, in the attempt to reproduce the experimental momentum profile by the weighted sum of theoretical predictions for the *trans*- and *cis*-geometries, no weighting factor could be identified that can reasonably explain the experimental results of all three ionization bands simultaneously.

Influence of the CC torsional motion

In order to infer the distribution of conformations with different φ values, the potential energy curve along the O=C-C=O dihedral coordinate has been constructed by plotting the energies obtained from a series of restricted geometry optimizations in which φ is kept constant. It has been reported that the potential energy curve of dimethyl oxalate exhibits significant sensitivity to the theoretical approach employed, owing to a delicate balance between two factors: the π-conjugation effect between the C=O groups and lone pair-lone pair repulsion. [8,9] The calculations were thus conducted at two different levels: the MP2 method and the DFT approach with the B3LYP functional. The aug-cc-pVTZ basis set was utilized in the calculations. The results are depicted in Fig. 4. The figure also presents the potential energy curve reported in a GED study. [9] This curve was inferred so as to maximize the reproduction of the gas-phase electron diffraction data based on a dynamic model. It is evident that there are substantial discrepancies among the potential energy curves. However, in all cases, the energy relative to the minimum value is either smaller than or comparable to the thermal energy at room temperature, ~207 cm^{-1}, across the majority of the dihedral angle range. Consequently, it is anticipated that the internal rotation around the CC bond leads to the variation of φ from 0° to 180°, and its influence should be taken into account in the data analysis.

View Article Online
DOI: 10.1039/D5CP00868B

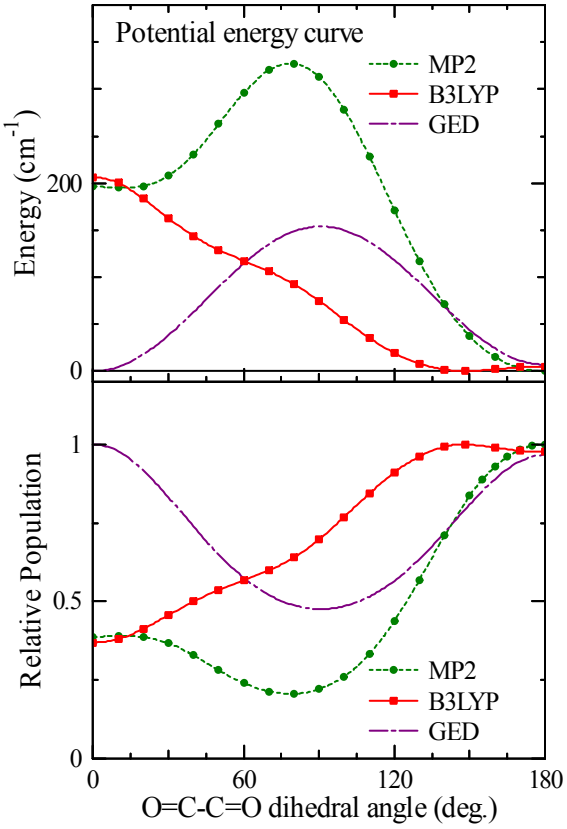

Fig.4 The potential energy curves of dimethyl oxalate along the O=C-C=O dihedral angle (top panel) and dihedral-angle distributions derived from these curves, with a temperature of 298 K (bottom panel). The theoretical results at the MP2 and B3LYP levels are represented as dashed lines with filled circles and solid lines with filled squares, respectively. The chain lines are result of the GED study by Vishnevskiy *et al.*[9]

In order to ensure the reliability of the analysis, it is necessary to incorporate not only the influence of the internal rotation around the CC bond but also the contributions of other vibrational modes. Within the HAQM approach, the influences of molecular vibration have been calculated under the assumption that the molecular structure varies in the vicinity of a well-defined equilibrium geometry due to internal vibrations.[32-38] However, the method cannot be directly applied to the present case, as the molecular structure undergoes significant change over a wide range of φ, and the vibrational effect may notably change with the angle. To address this issue, an adiabatic approximation is introduced as described below.

The internal motion with changing φ corresponds to the torsional vibration around the CC bond. The normal mode analysis indicates that the frequency of the CC torsional vibration is in a few tens of cm^{-1}, and the energy separation between the neighboring vibrational levels is significantly lower than the thermal energy at room temperature. Accordingly, the φ distribution can be adequately described by the following Boltzmann distribution:

$$P(\varphi;T) = \exp\left[\frac{-V(\varphi)}{k_B T}\right] \Big/ Z ,$$

where k_B and Z represent the Boltzmann constant and the partition function, respectively, and $V(\varphi)$ denotes the potential energy function along φ. The φ distributions at room temperature are illustrated in the bottom panel of Fig. 4, with the maximum values being rescaled to 1. It is reasonable to hypothesize that the large-amplitude CC torsional motion is significantly slower compared to the other vibrational modes with higher frequencies. Within this assumption, the gradual change in the molecular geometry induced by the CC torsional vibration can be treated as adiabatically slow when considering the influence of the other vibrational modes. According to this adiabatic approximation, the results of the vibrational effects calculations conducted at each φ are averaged over the angle after weighting $P(\varphi; T)$ to obtain the momentum profiles that include the influences of both large-amplitude CC torsional motion and other vibration modes.

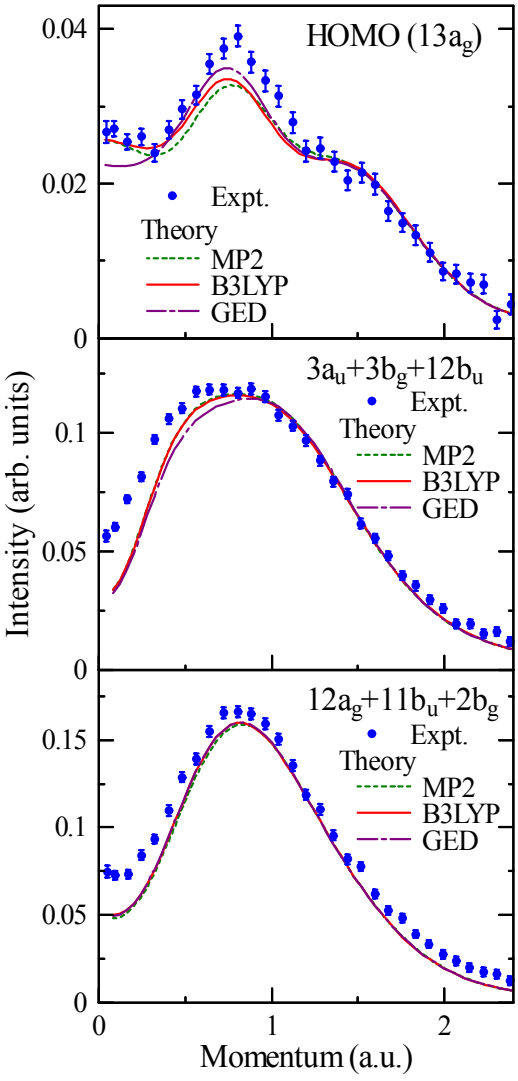

Fig. 5 Comparison of the experimental momentum profiles with theoretical calculations that incorporate the influence of the CC torsional motion at room temperature as well as the effect of other vibrational modes. The dashed, solid, and chain lines represent the theoretical results obtained using the MP2, B3LYP, and GED potential energy curves, respectively. All theoretical momentum profiles are folded with the instrumental momentum resolution.

Figure 5 compares the theoretical momentum profiles thus obtained using the three different $V(\varphi)$'s depicted in Fig. 4 with

Journal Name ARTICLE

View Article Online
DOI: 10.1039/D6CP00858B

the experiment. It is evident that all calculations have yielded substantial enhancements in the agreement with the experimental results, compared to the case assuming a fixed φ value. For the $13a_g$ orbital, the experiment exhibits a relatively uniform distribution up to p ~ 0.3 a.u., followed by a maximum at p ~ 0.8 a.u. These features are accurately reproduced by the theoretical results. Furthermore, the calculations demonstrate good accordance with the experimental outcomes for both the $\{3a_u + 3b_g + 12b_u\}$ and $\{12a_g + 11b_u + 2b_g\}$ orbitals. These findings clearly indicate that the structure of dimethyl oxalate distributes over a wide φ region at room temperature.

While the incorporation of the φ distribution effect into the calculation results in the reasonable agreement with the experimental momentum profiles, deviation from the experiment persists to some extent at p < ~0.5 a.u. for the $\{3a_u + 3b_g + 12b_u\}$ and $\{12a_g + 11b_u + 2b_g\}$ orbitals. One potential origin of the discrepancy is the distortion of the incoming and outgoing electron waves from plane waves (distorted-wave effect), which is caused by the target potential. [10] It has been established that the distorted-wave effect, which emerges when the incident electron energy is not sufficiently high to satisfy the PWIA, may enhance the intensity near p = 0 for orbitals that possess a d-orbital-like shape, such as a π^* orbital. [44-46] The $3a_u$, $3b_g$, and $2b_g$ orbitals exhibit a π antibonding character, thereby enabling the manifestation of the distorted-wave effect at small p in the $\{3a_u + 3b_g + 12b_u\}$ and $\{12a_g + 11b_u + 2b_g\}$ momentum profiles. An additional experiment was thus conducted at a lower incident electron energy of 0.8 keV to examine the distorted-wave effect. The results of the experiment are provided in the supplementary information. For the $13a_g$ orbital, the momentum profiles at E_0 = 0.8 and 1.2 keV are in agreement within the error bars, indicating the achievement of the high energy limit (see Fig. S2 in the supplementary information). In contrast, the $\{12a_g + 11b_u + 2b_g\}$ momentum profile at E_0 = 0.8 keV has exhibited higher intensity below p ~ 0.7 a.u. than that at E_0 = 1.2 keV. A similar tendency has been observed for the $\{3a_u + 3b_g + 12b_u\}$ momentum profile, though the change with E_0 is less distinct compared to the case of the $\{12a_g + 11b_u + 2b_g\}$ orbital. These findings indicate that the high energy limit is not attained at E_0 = 0.8 keV, suggesting the potential persistence of the distorted-wave effect even at E_0 = 1.2 keV for the second and third ionization bands. In the following, the focus is on the $13a_g$ orbital, for which the distorted-wave effect is deemed negligible.

A closer look at Fig. 5 reveals a small but discernable discrepancy between the theoretical momentum profiles of the $13a_g$ orbital. This can be attributed to the disparity between the potential energy curves employed in the calculations. In the vicinity of p = 0, the GED result exhibits lower intensity than the other theoretical predictions and considerably underestimates the experiment. Theoretical calculations for each φ have indicated that the $13a_g$ momentum profile of the planar *trans*-conformer (φ = 180°) displays a predominant maximum at p = 0 (see Fig. 3) and that the peak intensity diminishes with the reduction of φ until the angle reaches ~120°. For geometries with φ lower than 120°, a minimum has been observed at p = 0. The GED result demonstrates a shallow minimum at p ~ 0, while the experiment exhibits a local maximum at that point. It indicates that the contribution from *trans*-conformation has been notably underestimated in the GED result, which was obtained using a potential energy curve with close energies of the *cis*- and *trans*-conformations. It can be deduced from the finding that the energy of the *cis*-conformation is higher than that of the *trans*-conformation. Indeed, at p ~ 0, the experiment is in excellent agreement with the theoretical momentum profiles obtained from the potential energy curves at the MP2 and B3LYP levels, both of which indicate the energy at φ = 0° to be higher by 2×10^2 cm^{-1} than that at φ = 180° (see Fig. 4).

A comparison of the MP2 and B3LYP results reveals that the latter exhibits higher intensity than the former at p = 0.2–0.8 a.u. and aligns more closely with the experiment in that p region. However, the difference between the two theoretical momentum profiles is not significant, and furthermore, both exhibit an underestimation of the experiment in the p region from 0.64 to 1.12 a.u. beyond the error bars. Thus, it is not possible to draw a definitive conclusion about the validity of the theoretical potential energy curves solely from the present results.

Temperature dependence of the $13a_g$ momentum profile

Despite the substantial difference between the MP2 and B3LYP potential energy curves, the theoretical momentum profiles derived using these curves exhibit a high degree of similarity. It is conceivable that the averaging of the momentum profile over a wide φ range at room temperature smears out the dependence on the potential energy curve. In this case, conducting the experiment at a sufficiently low temperature can result in the enhancement of the difference between the momentum profiles obtained from the different potential energy curves. This is due to the fact that the molecular structure is concentrated around the bottom of the potential well, where a significant discrepancy between the MP2 and B3LYP results becomes evident. The execution of such an experiment is indeed possible through the employment of a supersonic molecular beam technique. In anticipation of future research endeavors focused on cooling molecules, a theoretical investigation is conducted to explore the temperature dependence of the $13a_g$ momentum profile.

The theoretical momentum profiles of the $13a_g$ orbital, calculated under the assumptions of T = 50, 100, and 298 K, are presented in Fig. 6. The temperature dependence is incorporated in the present model by the Brotzman distribution for the CC torsional angle, as well as $P_v(T)$ in eqn (2). The top panel of the figure displays the results obtained through the utilization of the MP2 potential energy curve, indicating that the intensity at p ~ 0 increases with decreasing temperature. A comparable temperature dependence has also been observed in the calculation employing the B3LYP potential energy curve, as illustrated in the middle panel of the figure. However, the extent of the increase in the intensity at p ~ 0 is considerably smaller than the calculation using the MP2 potential energy curve. This discrepancy is more clearly seen in the direct

comparison of the momentum profiles calculated for T = 50 K (depicted in the bottom panel). The MP2 calculation has predicted that the planar *trans*-geometry is the equilibrium geometry, and that the energy of the molecule rapidly increases with the decrease in φ from 180°. In contrast, the equilibrium geometry derived from the B3LYP calculation is at φ = 148.2°, and the potential energy curve exhibits a pronounced flatness over the range of 140° – 180° (see Fig. 4). The observed discrepancy between the two theoretical predictions can be attributed to the difference in the theoretical potential energy curves. The present result indicates that the EMS experiment at low temperature offers an opportunity to examine the potential energy curve. A study based on this idea is currently being planned in our group.

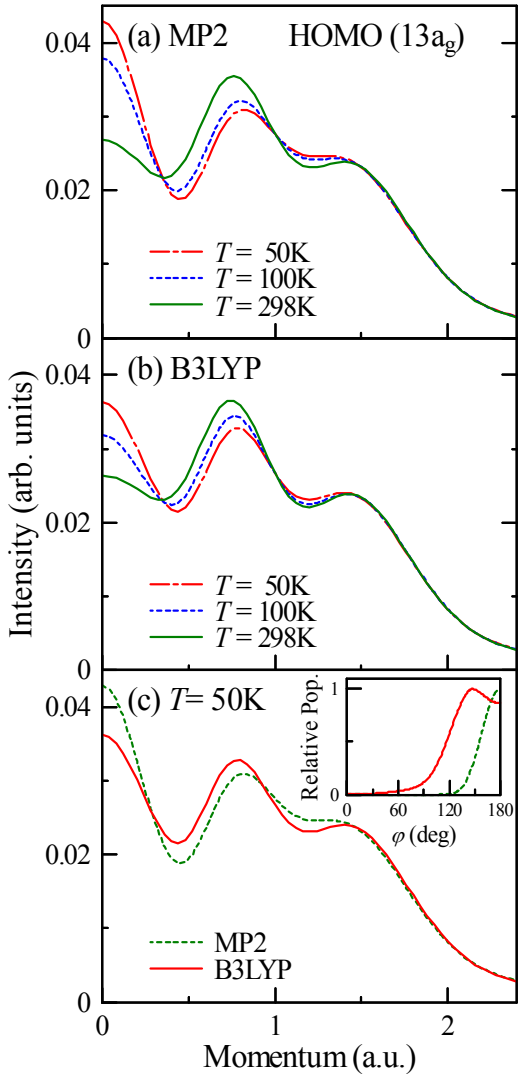

Fig. 6 Theoretical momentum profiles of the 13a$_g$ orbital at T = 50, 100, and 298 K, which were obtained using the potential energy curves at the (a) MP2 and (b) B3LYP levels. Panel (c) presents a comparison of the momentum profiles at T = 50 K obtained using the MP2 and B3LYP potential energy curves. The φ distributions derived from these curves are illustrated in the insert of panel (c).

Summary

EMS experiments were conducted on dimethyl oxalate in order to assess the efficiency of EMS in investigating molecular conformation. The experimental momentum profiles were then compared with theoretical calculations employing a series of molecular geometries that vary the CC torsional angle, φ. It has been revealed that the momentum profile of the 13a$_g$ orbital is highly sensitive to φ, and that the experimental outcomes cannot be adequately explained under the assumption of φ being fixed to a single value. In the light of this finding, an extension of the HAQM approach was introduced to incorporate the influence of both the large-amplitude CC torsional motion and other vibrational modes into the theoretical momentum profiles. Consequently, the deviation from the experiment has been almost resolved, indicating that φ varies from 0° to 180° at room temperature due to the internal rotation around the CC bond. A comparison of the experiment with the theoretical momentum profiles obtained using different potential energy curves demonstrates that the *trans*-structure possesses a lower energy than that of the *cis*-structure.

Theoretical explorations were subsequently conducted on the temperature dependence of the 13a$_g$ momentum profile, in anticipation of future research on structural flexible molecules cooled through the utilization of a supersonic molecular beam technique. The theoretical momentum profile of the 13a$_g$ orbital exhibited a considerable variation with temperature, and the difference between the results obtained using the MP2 and B3LYP potential energy curves was found to be enhanced with decreasing temperature. This finding suggests that the EMS experiment at low temperature provide a valuable opportunity to examine the CC torsional potential, whose prediction exhibits a considerable variation with the theoretical method employed.

The present study has demonstrated that EMS can be used to investigate molecular conformations that are challenging to be fully determined by conventional structure-analysis techniques. In particular, the extended HAQM approach based on the adiabatic approximation furnishes a foundation for the application of the EMS method to molecules that exhibit a high degree of flexibility along a torsional coordinate. Torsional potentials have been shown to play a pivotal role in the dynamical mechanisms of chemical reactions, [47] and have been an active subject of theoretical studies. [47,48] EMS may offer an experimental tool to investigate torsional potentials and the influence of torsional motion on electronic wavefunctions.

Author contributions

N. W.: conceptualization, investigation, formal analysis, visualization, writing–original draft. S. A.: investigation, formal analysis. M. T.: supervision, writing– review & editing.

Conflicts of interest

There are no conflicts to declare.

View Article Online
DOI: 10.1039/D6CP00868B

Data availability

The experimental and theoretical results supporting this article have been included within the article and the supplementary information. The supplementary information contains the binding energy spectrum and electron momentum profiles of dimethyl oxalate measured at an incident electron energy of 0.8 keV.

Acknowledgements

This research was supported by the JSPS KAKENHI Grant Numbers JP23K21091, JP25K01722 and JP25H00865.

References

1 M. W. Dougill and G. A. Jeffrey, *Acta Crystallogr.*, 1953, **6**, 831-837, DOI: 10.1107/S0365110X53002453.
2 J. P. Jones, B. A. Cornell, E. Horn and E. R. T. Tiekink, *J. Crystallogr. Spectrosc. Res.*, 1989, **19**, 715-723, DOI: 10.1007/BF01179844.
3 B. D. Saksena, Proc. *India Acad. Sci. Sect. A*, 1940 **12**, 416-427, DOI: 10.1007/BF03172589.
4 T. Miyazawa, *J. Chem. Soc. Jap.*, 1954, **75**, 540-544, DOI: 10.1246/nikkashi1948.75.540.
5 J. K. Wilmhurst and J. F. Horwood, *J. Mol. Spectrosc.*, 1966, **21**, 48-65, DOI: 10.1016/0022-2852(66)90121-4.
6 J. R. Durig and S. C. Brown, *J. Mol. Struct.*, 1976, **31**, 11-21, DOI: 10.1016/0022-2860(76)80114-7.
7 J. E. Katon and S.-L. Lin, *J. Mol. Struct.*, 1978, **48**, 335-342, DOI: 10.1016/0022-2860(78)87243-3.
8 S. B. Lopes, L. Lapinski and R. Fausto, *Phys. Chem. Chem. Phys.*, 2002, **4**, 1014-1020, DOI: 10.1039/B107232N.
9 Y. V. Vishnevskiy, A. A. Ivanov, H. Oberhammer and L. V. Vilkov, *Struct. Chem.*, 2005, **16**, 41-46, DOI: 10.1007/s11224-005-1079-y.
10 I. E. McCarthy and E. Weigold, *Rep. Prog. Phys.*, 1991, **54**, 789-879, DOI: 10.1088/0034-4885/54/6/001.
11 M. A. Coplan, J. H. Moore and J. P. Doering, *Rev. Mod. Phys.*, 1994, **66**, 985-1014, DOI: 10.1103/RevModPhys.66.1517.
12 M. Takahashi, *Bull. Chem. Soc. Jpn.*, 2009, **82**, 751-777, DOI: 10.1246/bcsj.82.751.
13 N. Watanabe, X. Chen and M. Takahashi, *Phys. Rev. Lett.*, 2012, **108**, 173201, DOI: 10.1103/PhysRevLett.108.173201.
14 N. Watanabe, M. Yamazaki and M. Takahashi, *J. Electron Spectrosc. Relat. Phenom.*, 2016, **209**, 78-86, DOI: 10.1016/j.elspec.2016.04.004.
15 N. Watanabe, K. Katafuchi, M. Yamazaki and M. Takahashi, *Eur. Phys. J. D*, 2016, **70**, 268, DOI: 10.1140/epjd/e2016-70516-7.
16 E. Wang, X. Shan, Q. Tian, J. Yang, M. Gong, Y. Tang, S. Niu and X. Chen, *Sci. Rep.*, 2016, **6**, 39351, DOI: 10.1038/srep39351.
17 M. S. Deleuze, W. N. Pang, A. Salam and R. C. Shang, *J. Am. Chem. Soc.*, 2001, **123**, 4049-4061, DOI: 10.1021/ja0039886.
18 S. Saha, F. Wang, C. T. Falzon and M. J. Brunger, *J. Chem. Phys.*, 2005, **123**, 124315, DOI: 10.1063/1.2034467.
19 M. S. Deleuze and S. Knippenberg, *J. Chem. Phys.*, 2006, **125**, 104309, DOI: 10.1063/1.220969.
20 F. Wu, X. Chen, X. Shan, S. X. Tian, Z. Li and K. Xu, *J. Phys. Chem. A*, 2008, **112**, 4360-4366, DOI: 10.1021/jp710757y.
21 M. Yan, X. Shan, F. Wu, X. Xia, K. Wang, K. Xu and X. Chen, *J. Phys. Chem. A*, 2009, **113**, 507-512, DOI: 10.1021/jp808281w.
22 Y. Shi, X. Shan, E. Wang, H. Yang, W. Zhang and X. Chen, *J. Phys. Chem. A*, 2014, **118**, 4484-4493, DOI: 10.1021/jp503198r.
23 Y. Tang, X. Shan, S. Niu, Z. Liu, E. Wang, N. Watanabe, M. Yamazaki, M. Takahashi and X. Chen, *J. Phys. Chem. A*, 2017, **121**, 277-287, DOI: 10.1021/acs.jpca.6b10009.
24 M. Takahashi, N. Watanabe, Y. Khajuria, K. Nakayama, Y. Udagawa, J. H. D. Eland, *J. Electron Spectrosc. Relat. Phenom.*, 2004, **141**, 83-93, DOI: 10.1016/j.elspec.2004.08.002.
25 A. D. Becke, J. Chem. Phys., 1993, **98**, 5648-5652, DOI: 10.1063/1.464913.
26 C. Lee, W. Yang and R. G. Parr, *Phys. Rev. B*, 1998, **37**, 785-789, DOI: 10.1103/physrevb.37.785.
27 P. Duffy, D. P. Chong, M. E. Casida and D. R. Salahub, *Phys. Rev. A*, 1994, **50**, 4707-4728, DOI: 10.1103/PhysRevA.50.4707.
28 A. O. Bawagan, C. E. Brion, E. R. Davidson and D. Feller, Chem. Phys., 1987, **113**, 19-42, DOI: 10.1016/0301-0104(87)80217-3.
29 M. J. Frisch, G. W. Trucks, H. B. Schlegel, G. E. Scuseria, M. A. Robb, J. R. Cheeseman,G. Scalmani, V. Barone, G. A. Petersson and H. Nakatsuji et al., Gaussian 16 Rev. C. 01, Wallingford, CT, 2016.
30 T. H. Dunning Jr., *J. Chem. Phys.*, 1989, **90**, 1007-1023, DOI: 10.1063/1.456153.
31 R. A. Kendall, T. H. Dunning, Jr. and R. J. Harrison, *J. Chem. Phys.*, 1992, **96**, 6796-6806, DOI: 10.1063/1.462569.
32 N. Watanabe, M. Yamazaki and M. Takahashi, *J. Chem. Phys.*, 2012, **137**, 114301, DOI: 10.1063/1.4752653.
33 N. Watanabe, M. Yamazaki and M. Takahashi, *J. Chem. Phys.*, 2014, **141**, 244314, DOI: 10.1063/1.4904705.
34 F. Morini, M. S. Deleuze, N. Watanabe and M. Takahashi, *J. Chem. Phys.*, 2015, **142**, 094308, DOI: 10.1063/1.4913642.
35 F. Morini, N. Watanabe, M. Kojima, M. S. Deleuze and M. Takahashi, *J. Chem. Phys.*, 2015, **143**, 134309, DOI: 10.1063/1.4931918.
36 Y. Tang, X. Shan, J. Yang, S. Niu, Z. Zhang, N. Watanabe, M. Yamazaki, M. Takahashi and X. Chen, *J. Phys. Chem. A*, 2016, **120**, 6855-6863, DOI: 10.1021/acs.jpca.6b06706.
37 N. Watanabe, K. Sato and M. Takahashi, *J. Chem. Phys.*, 2019, **150**, 194306, DOI: 10.1063/1.5097201.
38 D. G. Matalon, K. L. Nixon and D. B. Jones, *Int. J. Mol. Sci.*, 2025, **26**, 11729, DOI: 10.3390/ijms262311729.
39 N. Watanabe, K. Takahashi, K. Sato and M. Takahashi, *J. Phys. Chem. A*, 2020, **124**, 10258-10265, DOI: 10.1021/acs.jpca.0c08799.
40 N. Watanabe, K. Kume and M. Takahashi, *J. Electron Spectrosc. Relat. Phenom.*, 2022, **259**, 147240, DOI: 10.1016/j.elspec.2022.147240.
41 J. F. Stanton and J. Gauss, *J. Chem. Phys.*, 1994, **101**, 8938-8944, DOI: 10.1063/1.468022.
42 M. W. Schmidt, K. K. Baldridge, J. A. Boatz, S. T. Elbert, M. S. Gordon, J. H. Jensen, S. Koseki, N. Matsunaga, K. A. Nguyen, S. J. Su, T. L. Windus, M. Dupuis and J. A. Montgomery, *J. Comput. Chem.*, 1993, **14**, 1347-1363, DOI: 10.1002/jcc.540141112.
43 S. P. McGlynn and J. L. Meeks, *J. Electron Spectrosc. Relat. Phenom.*, 1976, **8**, 85-93, DOI: 10.1016/0368-2048(76)80011-4.
44 C. E. Brion, Y. Zheng, J. Rolke, J. J. Neville, I. E. McCarthy and J. Wang, *J. Phys. B: At. Mol. Opt. Phys.*, 1998, **31**, L223-L230, DOI: 10.1088/0953-4075/31/5/003.
45 X. G. Ren, C. G. Ning, J. K. Deng, S. F. Zhang, G. L. Su, F. Huang and G. Q. Li, *Phys. Rev. Lett.*, 2005, **94**, 163201, DOI: 10.1103/PhysRevLett.94.163201.

View Article Online
DOI: 10.1039/D6CP00868B

46 M. Gong, Y. Zhang, X. Li, S. B. Zhang, X. Shan and X. Chen, *Phys. Rev. A*, 2022, **105**, 042805, DOI: 10.1103/PhysRevA.105.042805.
47 D. N. Tahchieva, D. Bakowies, R. Ramakrishnan and O. A. von Lilienfeld, *J. Chem. Theory Comput.*, 2018, **14**, 4806-4817, DOI: 10.1021/acs.jctc.8b00174.
48 S. Nam, E. Cho, E. Sim and K. Burke, J. Phys. Chem. Lett., 2021, **12**, 2796-2804, DOI: 10.1021/acs.jpclett.1c00426.

View Article Online
DOI: 10.1039/D6CP00868B

Data availability

The experimental and theoretical results supporting this article have been included within the article and the supplementary information. The supplementary information contains the binding energy spectrum and electron momentum profiles of dimethyl oxalate measured at an incident electron energy of 0.8 keV.